Maneuver Detection for Cislunar Vehicles Using Optical Measurements

Jesse Greaves
University of Colorado Boulder
Daniel Scheeres
University of Colorado Boulder

ABSTRACT

The international interest in the sustained development of cislunar space will generate traffic and debris in the region as it has done near Earth. As a consequence there will be increased demand for cislunar situation awareness which has many challenges. Two primary issues to be addressed are observational strategies and maneuver detection. An observational strategy based around cislunar optical observers leverages existing technologies to alleviate Earth-based resources and provide robust estimation. Even with cislunar observational tools, estimation of desired objects can be easily lost due to the chaotic dynamics of the region. To improve estimation capabilities the ballistic Optimal Control Based Estimator (OCBE) can be utilized to identify unmodeled perturbations, and subsequently identified events can be statistically categorized using uncertainty quantification methods. This methodology not only yields reliable tracking, but also provides a statistical framework to label maneuvers. This methodology is simulated with observers at multiple cislunar locations to determine visibility properties, OCBE control policy distributions, and maneuver detection performance. These simulations both demonstrate the visibility challenges associated with optical observation in cislunar space and the advantages of the newly developed method for maneuver detection.

1. INTRODUCTION

There is great international interest in developing cislunar space for future exploration and exploitation. First and foremost, NASA's Moon to Mars program and Lunar Gateway project are exemplary of this growing interest since they plan to develop cislunar space into an outpost and highway for deep space exploration [3]. This vision suggests that there will be a myriad of spacecraft flying through cislunar space; everything from crewed vehicles to robotic explorers. NASA isn't alone in its vision for developing cislunar space though, with organizations such as JAXA, ESA, CNSA, Roscosmos, ISA, and ISRO having all publicly expressed interest in cislunar space [2]. This growing interest will lead to a surge in traffic, and inevitably, debris in the region. In order to ensure long-term use and safety for all cislunar vehicles the congestion on this interplanetary highway will need to be monitored carefully.

Estimating cislunar spacecraft is exacerbated by the chaotic dynamics of cislunar travel. Chaotic dynamics mean that small perturbations and estimation inaccuracies will lead to large predictive errors, which lead to filter divergence if unaccounted for or if not enough information is ingested into the system. These dynamics also mandate a station keeping scheme for all spacecraft, which will need to be separated from other maneuvers to maintain an understanding of system health [1]. If station keeping and other events aren't identified fast enough then the spacecraft will quickly deviate from the nominal and the track will be lost. This necessitates some form of maneuver detection for long-term estimation purposes.

Traditional high accuracy estimation methods for cislunar spacecraft are based around Earth-based radar measurements like the DSN [1]. While this can provide accurate solutions for cooperative vehicles, this leads to several problems for persistent observation. First, scheduling DSN time is difficult because it is already heavily subscribed. Second, the DSN isn't optimized for non-cooperative vehicles and therefore cannot provide the same level of accuracy for them. Third, only taking measurement from Earth severely limits viewing geometry which leads to limited observational capacity. In order to alleviate these issues cislunar observation platforms can be employed. By placing observers around cislunar space with optical measurement devices, persistent and accurate observation of cooperative and non-cooperative targets can be maintained.

These enabling geometries allows for accurate estimation of cislunar systems but does not account for maneuvering spacecraft. The Optimal Control Based Estimator (OCBE), which provides additional statistics that are sensitive to unmodeled forces, is then used to build optimal control policy distributions on training data. By creating an expected distribution of the OCBE statistics, a given system's maneuvers and health can be tracked to a much finer level, since being able to identify events enables accurate and robust estimation of cislunar spacecraft. Being capable of providing this consistent and robust tracking will reduce the uncertainty for cooperative and non-cooperative systems alike, ensuring the safety of all the systems in cislunar space.

2. PROBLEM DEFINITION

2.1 Dynamics Models

The Circular Restricted 3 Body Problem (CR3BP) approximates cislunar dynamics and trajectories found in the CR3BP hold with small deviations in higher fidelity models [7]. The equations of motion for the CR3BP, in their non-dimensional form and in the synodic frame, are given in Equation 1. The synodic frame is a frame that is fixed to the rotation of the 2 bodies such that the primary and secondary always lie on the x-axis. The z-axis is then aligned with the angular momentum of the system, and y-axis completes the frame. The origin of this frame is the center of mass of the system.

$$\ddot{r} = -2\hat{z} \times \dot{r} - \hat{z} \times (\hat{z} \times r) - \frac{1-\mu_g}{|r_1|^3} r_1 - \frac{\mu_g}{|r_2|^3} r_2 \tag{1}$$

There are 2 NRHOs used in this paper; an approximate 9:2 resonance orbit which NASA is targeting for its Lunar Gateway and a stable NRHO with a stability index of 1. Both are southern L2 NRHOs found using a standard single shooting algorithm with initial conditions at apoapsis. Because the initial condition is at apoapsis the initial y position, and x and z velocities are 0. The details of these orbits including the stability index, radius of periapsis, and non-dimensional non-zeros initial conditions are given in Table 1. These orbits and other family members are displayed in Figure 1. The 9:2 resonance orbit is highlighted in blue and the stable orbit is highlighted in red. Note the axis in Figure 1 are centered about the Moon's origin.

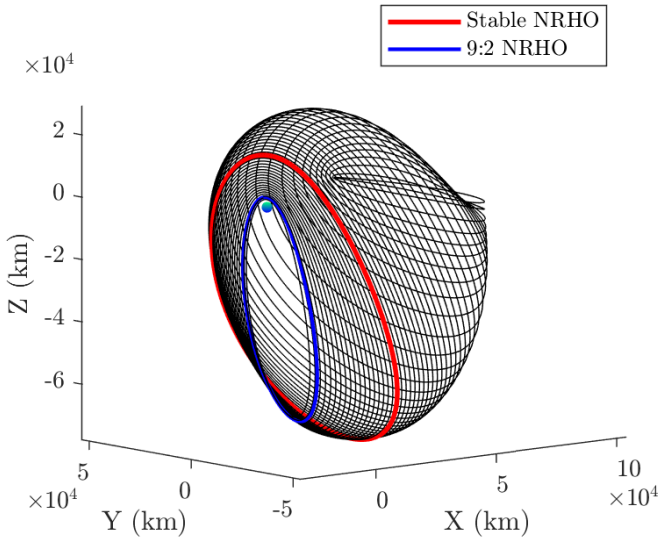

Fig. 1: NRHO family with 2 reference orbits highlighted in blue and red.

Table 1: NRHO Details

Orbit ID	Stability Index	R_p (km)	Initial Conditions (non-dim)		
			r_x	r_z	$\dot{r}_y$
9:2 Resonance	-1.320604	3236.299051	1.0219e+00	-1.8206e-01	-1.0309e-01
Stable	1.0	16428.054081	1.0796e+00	-2.0237e-01	-1.9739e-01

The station keeping model is based on previous NRHO station keeping work [7]. It shows that station keeping is best performed by burning at apoapsis every revolution. Due to the small station keeping costs it may be impractical, or impossible, to execute the minor burns every revolution. The station keeping costs vary dramatically with navigation errors but are capped by 5 m/s burns and are often on the order of 10's of mm/s. To approximate these station keeping maneuvers for uncertainty quantification purposes a randomly pointing impulse is added at apoapsis with a Gaussian magnitude truncated to 3 sigma. Within this framework there are 2 station keeping policies that are examined. First, an active policy with a mean of 1 m/s and standard distribution of 0.3 m/s. Then a quiet policy with a mean of 50 mm/s and a 15 mm/s standard distribution. This encapsulates most plausible station keeping impulses.

2.2 Measurement Models

The optical measurements are represented by azimuth and elevation angles provided by the observer. The measurements can either be processed on-board or sent back to Earth for processing since observing craft require communications with Earth to maintain its own accuracy. The equations for azimuth and elevation are given in Equations 3 and 4 respectively. Note that these equations only contain position information, which causes state estimation issues later.

$$\rho = r - r_{obs} \tag{2}$$

$$\theta = atan2(\rho_y, \rho_x) \tag{3}$$

$$\phi = asin(\frac{\rho_z}{|\rho|}) \tag{4}$$

The rates at which these angles change are analytically derived in by Equations 6 and 7. These angular rates contain velocity information and are therefore extremely valuable measurements. It is assumed that some form of optical differentiation is performed to provide this information.

$$\dot{\rho} = \dot{r} - \dot{r}_{obs} \tag{5}$$

$$\begin{aligned} \dot{\theta} &= \frac{1}{(\rho_y/\rho_x)^2+1}\left(\frac{\dot{\rho}_y}{\rho_x} - \frac{\rho_y\dot{\rho}_x}{\rho_x^2}\right) \\ &= \frac{\rho_x\dot{\rho}_y - \rho_y\dot{\rho}_x}{\rho_y^2+\rho_x^2} \end{aligned} \tag{6}$$

$$\begin{aligned} \dot{\phi} &= \frac{1}{(1-(\rho_z/|\rho|)^2)^{1/2}}\left(\frac{\dot{\rho}_z}{|\rho|} - \frac{\rho_z|\dot{\rho}|}{|\rho|^2}\right) \\ &= \frac{1}{(1-(\rho_z/|\rho|)^2)^{1/2}}\left(\frac{\dot{\rho}_z}{|\rho|} - \frac{\rho_z(\rho\cdot\dot{\rho})/|\rho|}{|\rho|^2}\right) \\ &= \frac{\dot{\rho}_z|\rho| - \rho_z(\hat{\rho}\cdot\dot{\rho})}{|\rho|(|\rho|^2-\rho_z^2)^{1/2}} \end{aligned} \tag{7}$$

The simplest form of differentiation that can be performed would be to take several successive observations and calculate angular change over the measurement time span according to a rule like the midpoint rule. Errors in the numeric angular rate estimate taken this way would primarily be an artifact of angular measurement precision and the time between measurements. It is assumed for the purpose of this paper that numerical errors associated with calculating the angular rate are negligible in comparison to the angular noise, and therefore the angular rate noise

comes from the 2 angular measurements used for the angular rate calculation. This means the angular rate noise is the sum of the 2 independent Gaussian angular measurements divided by the time between the 2 measurements. The angular rate measurements are also assumed to be processed outside the state estimator and made available to the filter. The measurement noise for all following simulations are given in Table 2.

Table 2: Measurement Noise

Angular Noise (rad)	Angular-Rate Noise (rad/s)
1e-6	$\sqrt{2}$e-6

A natural placement for a cislunar observer would be in the vicinity of the L2 equilibrium point for its uninterrupted view of L2 NRHOs. Other attractive observer locations include the lunar surface or a Distant Retrograde Orbit (DRO). The spacecraft observers, such as the ones located at L2 and on the DRO, model lunar occultations. It was found that while the L2 observers doesn't experience visual outages, the DRO can have limited outages that are infrequent and short. The lunar surface observatories are limited by their horizon and therefore requires 3 observatories to view the full orbit 9:2 orbit due to its close periapsis. All observer locations and the NRHOs are displayed with respect to the Moon's center in Figure 2.

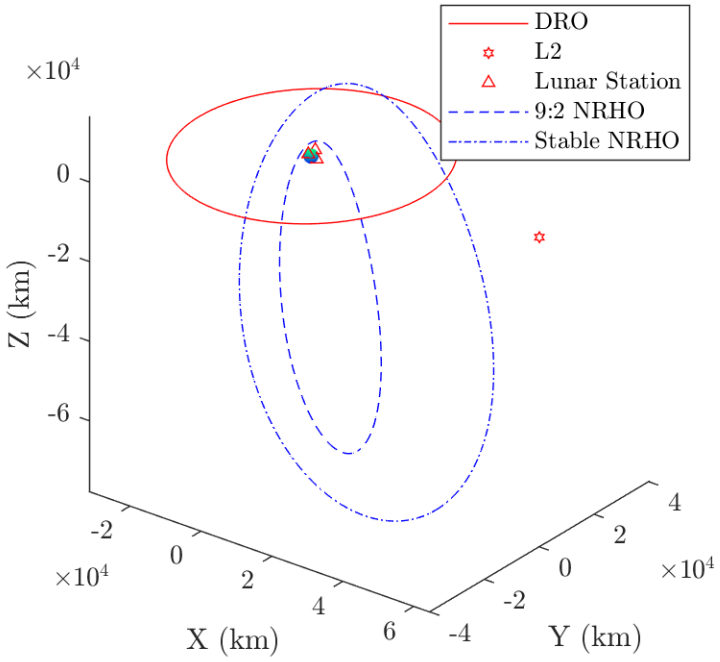

Fig. 2: Observer locations in red, and NRHOs in blue.

2.3 Maneuver Detection

The methodology for maneuver detection is to apply the OCBE to the estimation problem, integrate the estimated control policy from the OCBE over the viewing period, and preform a hypothesis test on the integrated control policy to determine if a maneuver has occurred. This effectively uses the total estimated thrust on the system for a hypothesis check against the expected thrust to identify maneuvers. The OCBE control policy's sensitivity to accelerations and thus makes this an ideal indicator of mismodeling, while its filtering properties act to remove noise and provide low variance results.

The ballistic OCBE is a generalized Kalman filter that provides an optimal control policy that dynamically connects measurement epochs which is then used as a control metric [5]. Control metrics measure the dynamic distance between update epochs, which provides more accurate event detection properties than state space distance metrics [4]. Because the OCBE is generalization of a Kalman filter it can be modified in the same manner as one. For this paper a square-root information version of the ballistic OCBE has been implemented to produce the desired filtering and optimal control profiles. The square-root information method used is from [6]. All relevant equations for the OCBE can be found in [5].

While the optimal control policy is useful for identifying maneuvers, it is often non-intuitive. Beyond that, in order to perform hypothesis tests there must be a known distribution for the desired quantity over the variable inputs. To better understand the optimal control policy its distribution must be numerically approximated via some uncertainty quantification method. The uncertainty quantification method of choice for this paper is Monte-Carlo. By running Monte-Carlo analysis of the integral of the control profile for maneuvering and non-maneuvering cases, unknown data sets can be tested against the known distributions to statistically determine where the unknown data most likely originated.

3. RESULTS

All results and simulations begin with an initial error and uncertainty dictated by Earth-radar observing. To match previous NRHO navigation studies the 3-sigma position uncertainty is 10 km and the velocity uncertainty is 10 cm/s [7]. This is to approximate SSA hand-off, or seeding, from the Earth-based resources to an optical observer as it unburdens its load.

For the following observation strategy studies simulations start at apoapsis due to estimation issues at periapsis. Starting at apoapsis gives the filter the best chance to reduce errors before arriving at periapsis. Once the filter failure issues have been addressed all other simulations start at perisapsis as to allow for error reduction before station keeping maneuvers. To save computation time a Monte Carlo analysis was run to determine the mean uncertainty of the system 3.5 hours before apoapsis, which is nearly deterministic, and that uncertainty was then used to seed the following control policy distribution and maneuver detection results.

3.1 Observation Strategy

Before the maneuver detection methodology can be applied, a viable observation strategy must be implemented. First, a simple angle only measurement scheme from the L2 observer was implemented. Measurement frequencies were varied from 30 minutes to 6 hours, but every strategy lead to constant filter divergence near periapsis for both the 9:2 and stable NRHOs.

In an attempt to constrain the system with additional geometric and rate information the L2 observer was supplemented with a DRO observer and lunar stations with measurements taken every hour from each observer. Even with this additional information the unstable 9:2 NRHO filter still always failed. The stable NRHO also commonly failed around periapsis but would occasional reconverge to the correct solution by the end of the orbit. This reconvergence was inconsistent and isn't reliable for robust observation. An example of the typical 9:2 NRHO filter divergence failure with all 5 observers is in Figure 3.

To provide velocity information to the filter angular rate measurements were added. A new tracking strategy using the single L2 observer with measurements taken every hour, now with angular and angular rates measurements, was implemented. Using this strategy it was found that both the 9:2 and stable NRHO states were easily estimated. Varying measurement frequencies from 30 minutes to 6 hours had minimal impact on the filters state estimation performance. This demonstrates the need to include angular rate information for cislunar estimation. A typical successful filter results is plotted in Figure 4.

To account for the station keeping maneuvers at apoapsis, process noise was added for a 7 hour window around apoapsis and simulated with a large station keeping maneuver. This still generated a convergent solution, and this information was smoothed to provide an improved optimal control profile. A typical result for a simulation with a station keeping maneuver and smoothing is plotted in Figure 5.

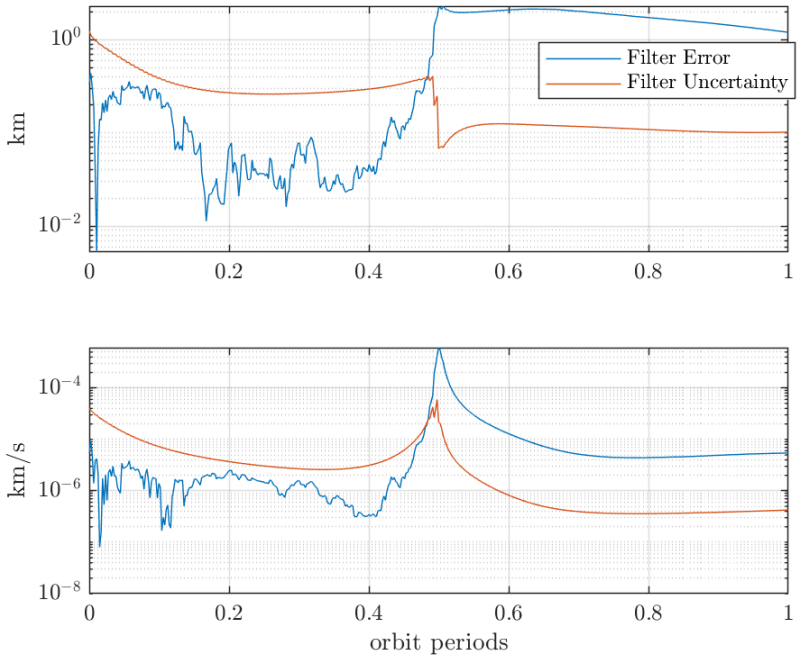

Fig. 3: Typical filter divergence with angle only measurements from L2, DRO, and lunar surface observers on the 9:2 NRHO starting at apoapsis.

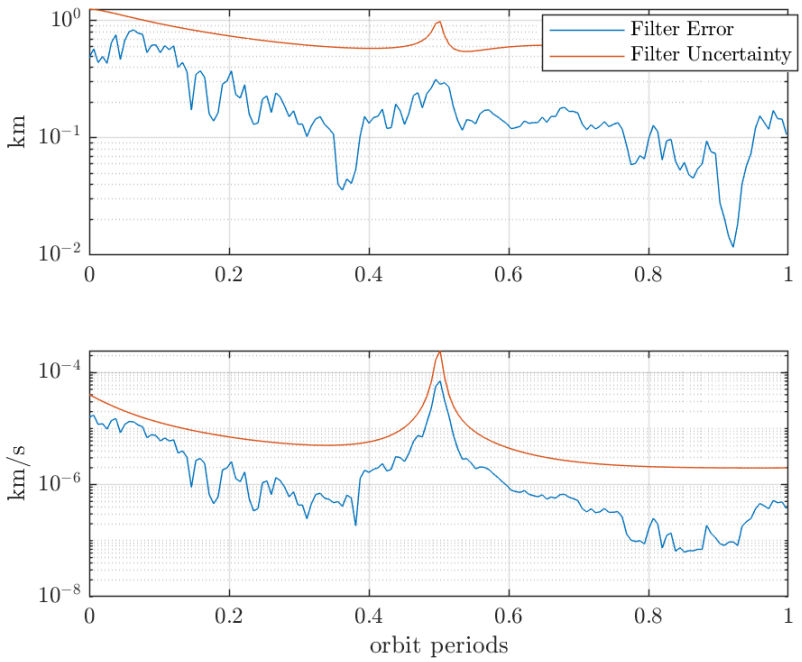

Fig. 4: Filter convergence with angular and angular rate measurements on the 9:2 NRHO starting at apoapsis.

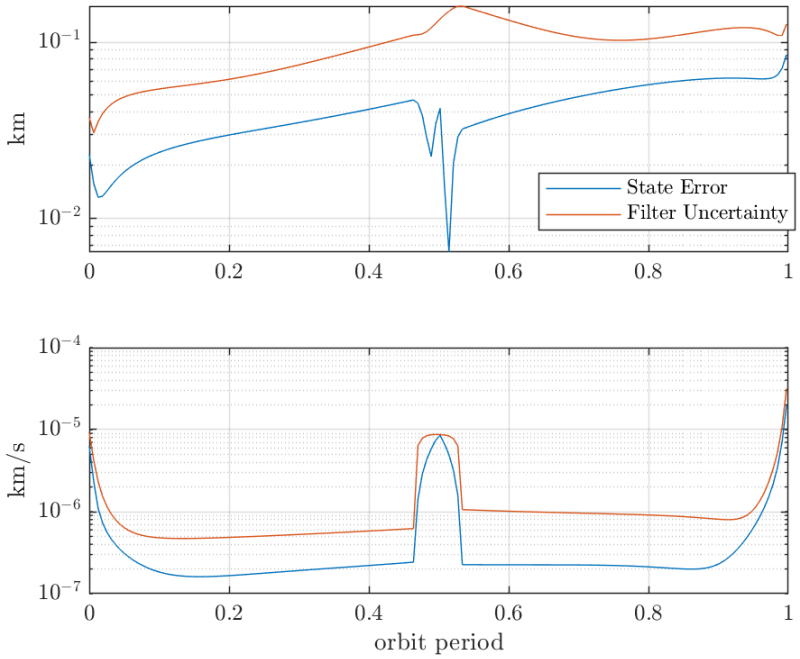

Fig. 5: Filter convergence with angular and angular rate measurements and a station keeping maneuver on the 9:2 NRHO starting at periapsis.

This exemplifies the estimation strategy for all future simulations. An Earth-based radar estimate is handed off to the optical observer at periapsis, where the system is observed for a single orbit period from a L2 observer with angular and angular rate measurements. A measurement cadence of 1 observation per 3 hours is adopted as a middle of the road frequency with accurate state estimation and maneuver detection abilities. Process noise is also added over a 7 hour window at apoapsis to account for maneuvers. An observer can use this strategy to maintain custody of the craft for an indefinite time as it performs station keeping maneuvers.

3.2 Control Policy Distribution

To perform a maneuver hypothesis tests the optimal control policy distribution for a given event must be numerically approximated via Monte-Carlo analysis. The variable input is the 3D station keeping maneuver which is modeled as a randomly pointing vector with a truncated Gaussian magnitude. The output of interest is the scalar integral of the control policy. Since it is desirable to identify both maneuvering and non-maneuvering craft a distribution is approximated for both cases. Non-maneuvering Monte-Carlo simulations only contain 500 runs, while maneuvering simulations contain 3000 runs to account for the variability in direction and size of the input. The control policy integrals are scaled by the mean of the non-maneuvering Monte-Carlo results to make the results more readable.

Over these Monte-Carlo runs it is likely the filter may fail occasionally due to the randomly generated initial errors and measurement outliers. But these runs are easily identified as they produce optimal control policies inconsistent with the vast majority of the results and can be re-run with an altered initial condition or identified measurement outliers to remedy the run. This is another advantage of approximating the control policy distribution that is utilized for these results.

Beginning with the active station keeping policy with a mean maneuver size of 1 m/s and standard deviation of 0.3 m/s it is clear that non-maneuvering systems produce statistically smaller control policies than maneuvering systems. The histograms of the control policy integrals for the 9:2 NRHO are in Figure 6. A PDF for these distributions are numerically calculated using Matlab's ksdensity function and overlaid on the histogram. A scatter plot of the maneuvering Monte-Carlo results are displayed in Figure 7 to show how the control policy varies with direction and magnitude. The stable NRHO produced similar results to the 9:2 NRHO.

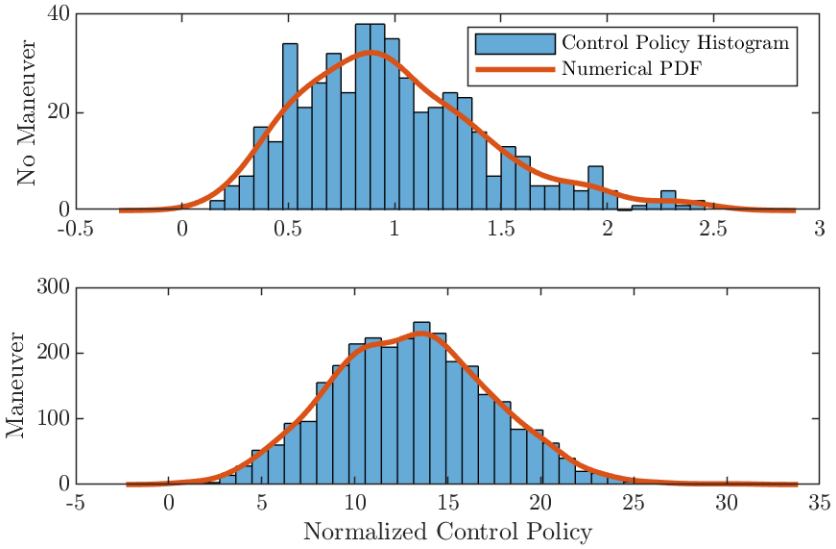

Fig. 6: Histogram and numerical PDF of Monte-Carlo results for 1 m/s mean non-maneuvering (top) and maneuvering case (bottom).

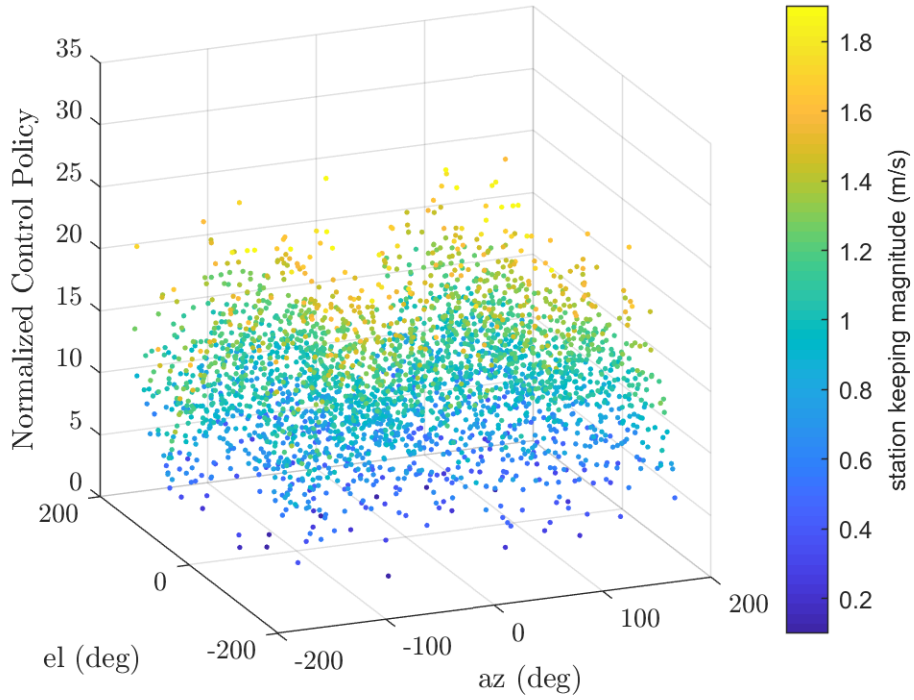

Fig. 7: Scatter of Monte-Carlo results for 1 m/s mean maneuvering case over input parameters.

The quiet station keeping policy with a mean maneuver size of 50 mm/s and standard deviation of 15 mm/s produced distributions with a significantly more overlap. The histograms of the control policy integrals for the 9:2 NRHO and overlaid numerical PDF are in Figure 8. A scatter plot of the maneuvering Monte-Carlo results is displayed in Figure 9 to show how the control policy varies with direction and magnitude. Once again, the stable NRHO produced similar results to the 9:2 NRHO.

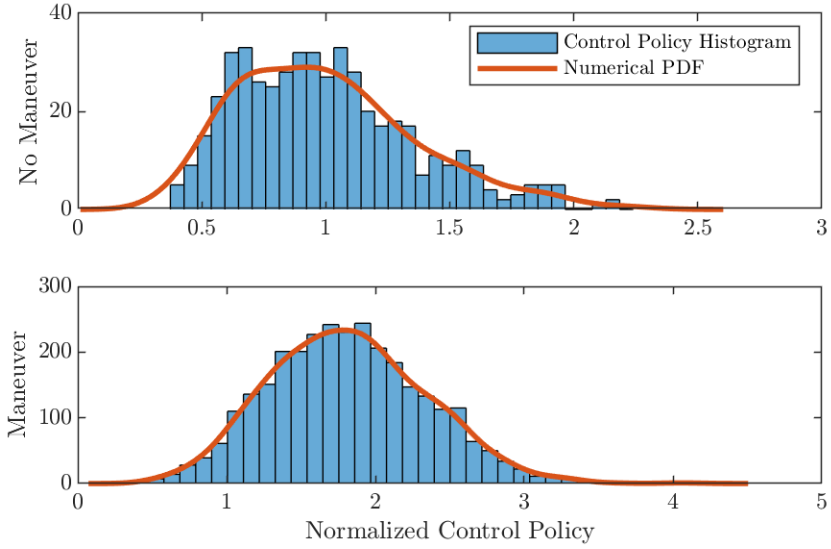

Fig. 8: Histogram and numerical PDF of Monte-Carlo results for 50 mm/s mean non-maneuvering (top) and maneuvering case (bottom).

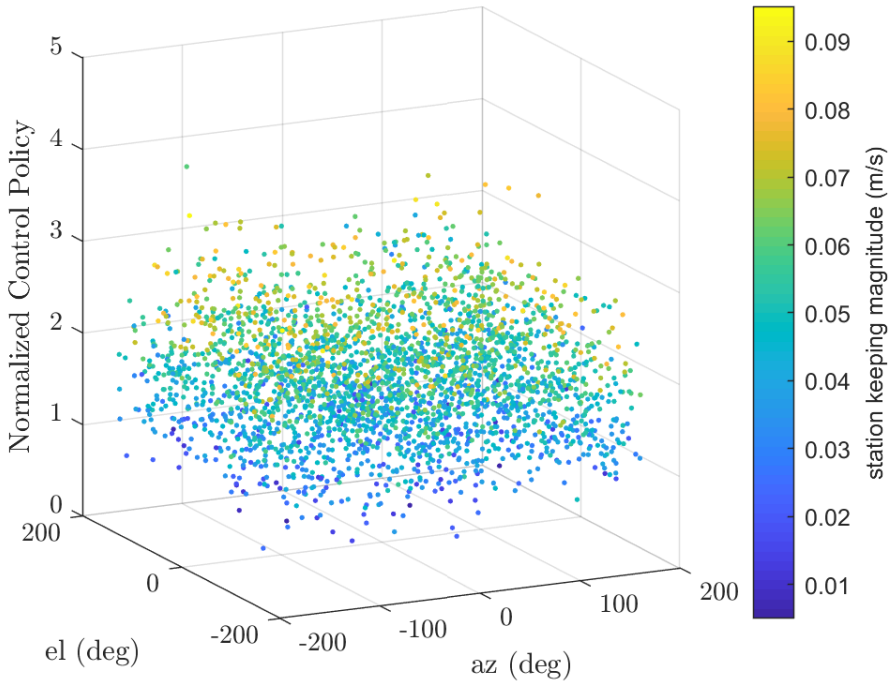

Fig. 9: Scatter of Monte-Carlo results for 50 mm/s mean maneuvering case over input parameters.

3.3 Maneuver Detection

With the OCBE control policy distributions approximated test data with unknown maneuvers can now be examined. To determine whether or not a maneuver occurred the test data's optimal control policy is evaluated against the numerical PDF of the maneuvering distribution and non-maneuvering distribution. The distribution that scores higher is the resulting estimate of whether or not a maneuver occurred.

100 maneuvering and 100 non-maneuvering data sets were generated for both the active and quiet station keeping policies, and the integrated control policy from the unknown data was tested for maneuvers. For the 9:2 NRHO with active station keeping, the maneuver tests returned an accuracy of 100%, and with quiet station keeping the maneuver tests returned an accuracy of 77%. The full results are in Table 3. The stable NRHO had a marginally better performance and the results for the stable NRHO are in Table 4.

Table 3: 9:2 NRHO Maneuver Detection Results

	Active ($\mu = 1m/s, \sigma = 0.3m/s$)		Quiet ($\mu = 50mm/s, \sigma = 15mm/s$)	
	No Maneuver	Maneuver	No Maneuver	Maneuver
Maneuver Identified	0	100	26	80
No Maneuver Identified	100	0	74	20

Table 4: Stable NRHO Maneuver Detection Results

	Active ($\mu = 1m/s, \sigma = 0.3m/s$)		Quiet ($\mu = 50mm/s, \sigma = 15mm/s$)	
	No Maneuver	Maneuver	No Maneuver	Maneuver
Maneuver Identified	0	100	15	76
No Maneuver Identified	100	0	85	24

4. CONCLUSION

Cislunar SSA is crucial to maintain the safety of all spacecraft going to the Moon and beyond. This task comes with a variety of challenges and is exasperated by limited Earth-based resources and chaotic dynamics. It has been shown that angular rate information is critical to the success of state estimation, but given angular rate measurements only a single observer is necessary to provide accurate observation. While having a L2 observer with angular and angular rate information enables a solution it doesn't account for the expected station keeping and other maneuvers that vehicles are likely to experience. The OCBE's control policy can be used to accurate identify maneuvers down to a 50 mm/s mean and 15 mm/s standard distribution. Future work must be down to adapt these results to higher fidelity simulations and identify smaller maneuvers.

[1] Diane Davis, Sagar Bhatt, Kathleen Howell, Jiann-Woei Jang, Ryan Whitley, Fred Clark, Davide Guzzetti, Emily Zimovan, and Gregg Barton. Orbit maintenance and navigation of human spacecraft at cislunar near rectilinear halo orbits. *27th AAS/AIAA Space Flight Mechanics Meeting*, 2017.

[2] Jeff Foust. International and commercial interest in the moon. The Space Review, 2017.

[3] Tracy Gill. Nasa's lunar orbital platform-gatway. *The Space Congress*, 2018.

[4] Marcus J Holzinger, Daniel J Scheeres, and Kyle T Alfriend. Object correlation, maneuver detection, and characterization using control distance metrics. *Journal of Guidance, Control, and Dynamics*, 35(4):1312–1325, 2012.

[5] Daniel P Lubey and Daniel J Scheeres. *Combined optimal control and state estimation for the purposes of maneuver detection and reconstruction*. PhD thesis, University of Colorado Boulder, 2014.

[6] Bob Schutz, Byron Tapley, and George H Born. *Statistical orbit determination*. Elsevier, 2004.

[7] Jacob Williams, David E Lee, Ryan J Whitley, Kevin A Bokelmann, Diane C Davis, and Christopher F Berry. Targeting cislunar near rectilinear halo orbits for human space exploration. *27th AAS/AIAA Space Flight Mechanics Meeting*, 2017.